Model of exchange-field penetration in nanocrystalline $Fe_{87}Zr_6B_6Cu$ alloys from magnetic and Mössbauer studies

J. S. Garitaonandia, D. S. Schmool, and J. M. Barandiarán
Departamento de Electricidad y Electrónica, Facultad de Ciencias, Universidad del País Vasco/EHU, Apartado 644, E-48080, Bilbao, Spain

(Received 29 December 1997; revised manuscript received 19 May 1998)

Magnetic measurements, x-ray diffraction, and Mössbauer spectroscopy have been used to study the structural and magnetic changes produced by annealing $Fe_{87}Zr_6B_6Cu$ amorphous alloys during the nanocrystallization process. Thermal annealing causes a devitrification of the amorphous phase giving rise to Fe crystallites in an amorphous remaining matrix. The amorphous phase shows an enhancement of the Curie temperature (T_c) and large changes in the hyperfine-field distribution [$P(B_{hf})$] in the presence of the crystallites. This is caused by compositional changes of the amorphous phase and exchange-field penetration from the Fe crystallites. A model, based on an exponential decay of the exchange field into the remaining amorphous phase and a distribution of the crystallites in a regular cubic array, is proposed to evaluate the effects of the exchange-field penetration on the T_c and $P(B_{hf})$. The model is applied to the partially crystallized $Fe_{87}Zr_6B_6Cu$ and to data on $Fe_{77}B_{18}Nb_4Cu$ taken from the literature. Quantitative agreement between the model and the average Curie temperature of the amorphous matrix is found. Changes of the coercive field with the annealing temperature in the nanocrystalline samples have also been evaluated within the model. Variations of the hyperfine-field distribution in the amorphous phase are discussed in terms of exchange-field penetration and compositional inhomogeneities. [S0163-1829(98)03341-4]

I. INTRODUCTION

Since Yoshizawa *et al.*[1] reported the excellent soft magnetic properties of partially crystallized Fe-rich nanocrystalline materials, great effort has been made in order to find the best materials and crystallization procedures to improve their magnetic properties. These materials, typically FeSiNbCuB and FeZrCuB amorphous alloys, present at least two different, well defined crystallization stages.[2–4] In the first stage an Fe-based phase crystallizes: DO_3-FeSi in FeSiNbCuB and α-Fe in the FeZrCuB alloys. As the first stage of crystallization does not present any overlap with the second stage, a partial crystallization of these alloys produces a nanocrystalline structure, where the grains are isolated from one another by an amorphous ferromagnetic matrix.

The excellent magnetic properties of these materials are due to the exchange coupling of the nanocrystals via the amorphous matrix which averages out and suppresses the macroscopic magnetic anisotropy.[5] An important consequence of such interactions is the increase in coercivity (H_c) when the temperature is raised above the Curie temperature (T_c) of the amorphous matrix and the changes of the magnetic properties of the amorphous phase produced by the presence of the crystallites. For example, Curie temperatures which are higher than those corresponding to the actual composition have been observed for the amorphous phase in partially crystallized Fe(Si)NbCuB.[6,7] The magnetic properties of the nanocrystals are also affected by their small size and the surrounding amorphous matrix, which has a lower magnetization than the bulk crystals, when the crystalline fraction is larger.[4,8] The theoretical explanation of many of these properties is related to the exchange coupling between the amorphous phase and the nanocrystals, and to exchange-field penetration from the latter into the former. Hernando *et al.*[6] have proposed an exponential decrease of the molecular field of the nanocrystals in the amorphous matrix, which explains the ''average behavior'' observed in H_c and T_c. Such effects are additional to the compositional and structural changes observed in the amorphous matrix upon nanocrystallization.

Studies which have so far reported on the exchange penetration of the nanocrystals into the amorphous matrix have been performed mainly by means of macroscopic measurements, such as coercivity or average Curie temperature. A microscopic technique such as Mössbauer spectroscopy can give detailed insight, on the atomic level, of these effects. Several works have been reported on nanocrystalline FeSiNbCuB (FINEMET type) alloys using Mössbauer spectroscopy.[4,9–11] However, the complexity of their spectra, due to the different Fe positions present in the DO_3 FeSi structure, obscures other interesting effects such as the importance of an interphase region or the exchange-field penetration in the amorphous matrix. The latter is also difficult to ascertain due to the relatively high Curie temperature of the amorphous phase in these alloys. In the FeZrCuB alloys, the nanocrystalline phase is quite simple: α-Fe. Moreover, the Curie temperature of the amorphous phase in these alloys is very close to room temperature, so any interaction or magnetic change can be easily resolved by Mössbauer spectroscopy. Magnetic measurements around the T_c of the amorphous matrix are also easier and there is no risk of further crystallization during the measurements. Thus, FeZrCuB presents a better system for investigating such effects.

The aim of this work is a detailed study of the structural and magnetic properties of $Fe_{87}Zr_6CuB_6$ nanocrystalline al-

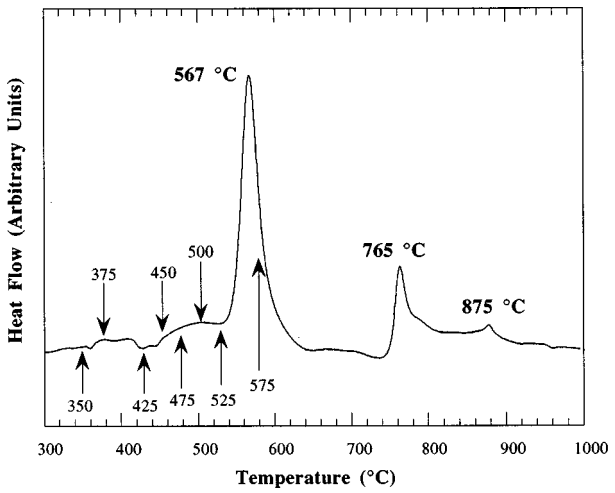

FIG. 1. DTA curve of the amorphous $Fe_{87}Zr_6B_6Cu$ sample.

loys, and, in particular, the exchange coupling between the nanocrystals and the amorphous matrix, from the early stages of the crystallization. In this paper Mössbauer and magnetic measurements, giving the Curie temperature distribution in the amorphous matrix, are reported. A second paper will deal with the interpretation of ferromagnetic resonance experiments on the same samples.[12]

II. EXPERIMENTAL

FeZrCuB amorphous ribbons were obtained by the melt spinning technique under a controlled atmosphere. In order to determine the best heat treatments to obtain a wide range of partial crystallizations, a calorimetric scan was performed using a differential thermal analyzer (DTA) at heating rate of 20 °C min^{-1}. Figure 1 shows the heat flow curve vs temperature and exhibits two different crystallization processes at temperatures of 567 and 765 °C. The first of them is associated with the crystallization of the α-Fe in a nanocrystalline state. So, one hour isothermal treatments at 350, 375, 425, 450, 475, 500, 525, and at 575 °C (where the first crystallization process has finished) were performed in the DTA apparatus in an Ar atmosphere.

The state of the crystallization in the samples was determined by x-ray diffraction (XRD) using Cu $K\alpha$ radiation. The peaks corresponding to an α-Fe polycrystalline foil were also used to obtain the instrumental corrections. The data obtained by this technique allows the identification of the different crystalline phases as well as the average grain size diameter and the lattice parameter of the α-Fe phase.

Magnetic measurements below 400 K were performed in a Quantum Design superconducting quantum interference device magnetometer. We have obtained the evolution of the magnetization with the temperature of the samples at 5 G in order to reduce, as much as possible, the effect of the applied field. Magnetization measurements above 400 K were obtained with a Manics DSM-8 Faraday magnetometer with an external field of 800 G.

Mössbauer spectroscopy was performed at room temperature in the transmission geometry using a conventional constant-acceleration spectrometer with a ^{57}Co-Rh source. Because of the sensitivity of the spectra to temperature changes (which is due to the closeness of T_c of the amorphous phase to room temperature) special care was taken in order to maintain a constant temperature (290 ± 0.5 K) during all experiments.

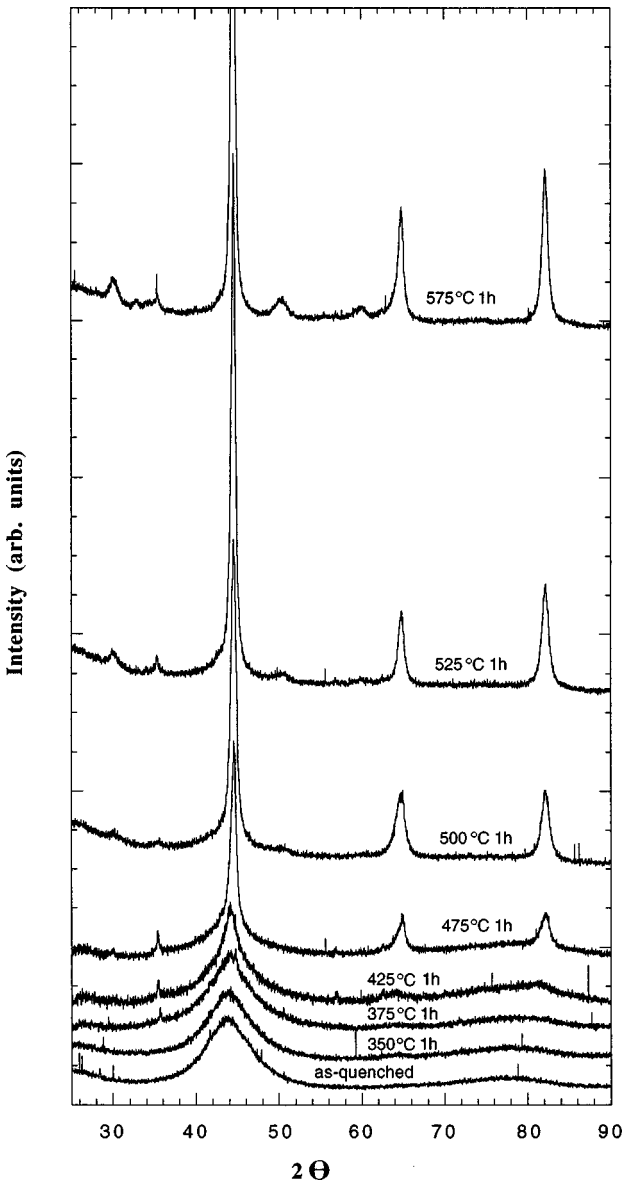

FIG. 2. X-ray diffraction patterns for the samples in the as-quenched state and isothermally annealed for one hour, annealing temperatures are indicated.

III. RESULTS

A. X-ray measurements

Figure 2 shows the x-ray diffraction (XRD) patterns of the as-quenched and annealed samples. In the diffraction pattern corresponding to the as-quenched sample and that at annealed at 350 °C, there is no evidence of any crystal line reflections. Only two broad halos, characteristic of the amorphous materials are present. In the pattern of the sample annealed at 375 °C, the narrowing of the main halo and the shoulder at $2\theta = 65°$, corresponding to the (200) α-Fe peak, indicate that the Fe crystallization process has begun. The crystallization is more evident in the diffraction pattern of the sample annealed at 425 °C: small peaks corresponding to

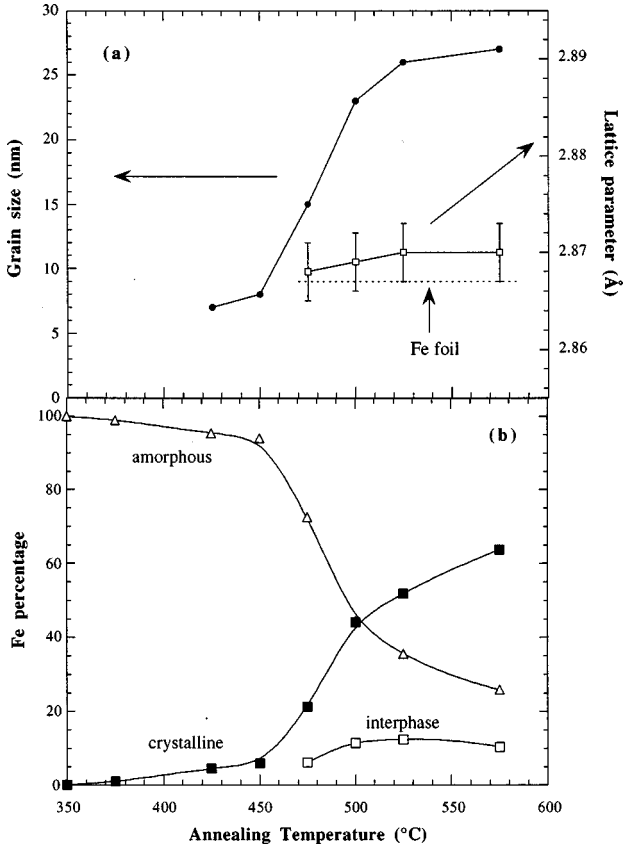

FIG. 3. (a) Variation of the grain size D and lattice parameter for the α-Fe crystallites as a function of the annealing temperature. (b) Relative percentage of iron in the crystalline, amorphous phase, and interphase regions as a function of the annealing temperature. The data has been determined from Mössbauer results.

the α-Fe bcc phase and a large amount of amorphous phase appear together.

For the samples annealed at higher temperatures these diffraction peaks become more intense, showing that the amount of crystalline phase is increasing at the expense of the amorphous phase. New small crystalline peaks appear for the samples annealed at 525 and 575 °C. These can be assigned to ZrO_2 (the reflection at about 30°) and iron-zirconium phases (Fe_3Zr, Fe_2Zr).[13,14]

The lattice parameter of the α-Fe phase has been calculated by means of the cos θ cotan θ method using the (110), (200), and (211) diffraction peaks,[15] and the grain size of the α-Fe crystals has been obtained from the width of the main peak, corresponding to the (200) reflection. The values are shown in Fig. 3(a).

B. Mössbauer measurements

In Figs. 4 and 5, we show the Mössbauer spectra along with the corresponding hyperfine field distributions for the samples from the as-quenched state to that annealed at 575 °C for 1 h.

The fitting of the Mössbauer spectra has been performed using the NORMOS program, developed by Brand *et al.*[16] This allows a simultaneous fit of several crystalline spectra with possible addition of an amorphous phase, which is characterized by a distribution of hyperfine fields B_{hf} with probability $P(B_{hf})$. The fittings have been performed using different procedures depending on state of crystallization in the samples.

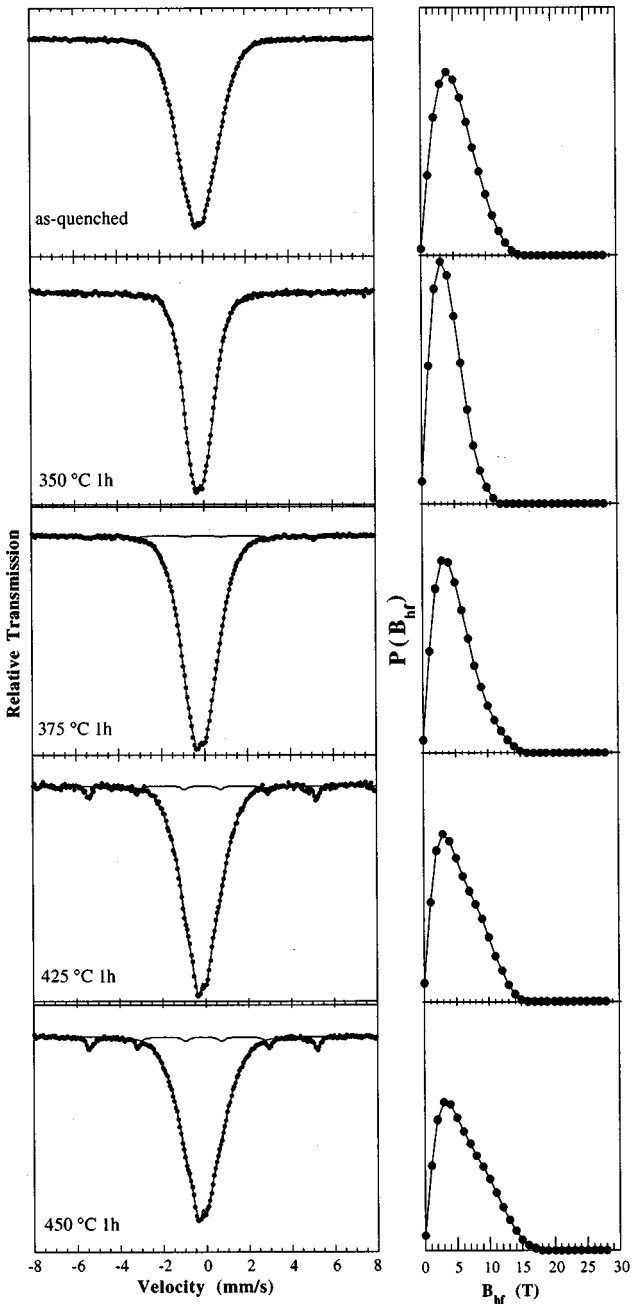

FIG. 4. Mössbauer spectra and fittings for the as-quenched sample and samples annealed at 350, 375, 425, and 450 °C. The corresponding hyperfine-field distributions are given on the right-hand side.

(a) In the Mössbauer spectra of the as-quenched sample and that annealed at 350 °C 1 h there is no evidence of crystallization, so a $P(B_{hf})$ has been used to fit both. These kinds of samples present typical asymmetries due to the correlation between the magnetic dipolar contribution and the electric field gradient[17] and due to the correlation between the local hyperfine field and the isomer shift (δ). In order to evaluate this correlation a linear relation between B_{hf} and δ in the distribution has been used:

$$\delta(B_j) = \delta(B_0) + \alpha(B_j - B_0) \quad (1)$$

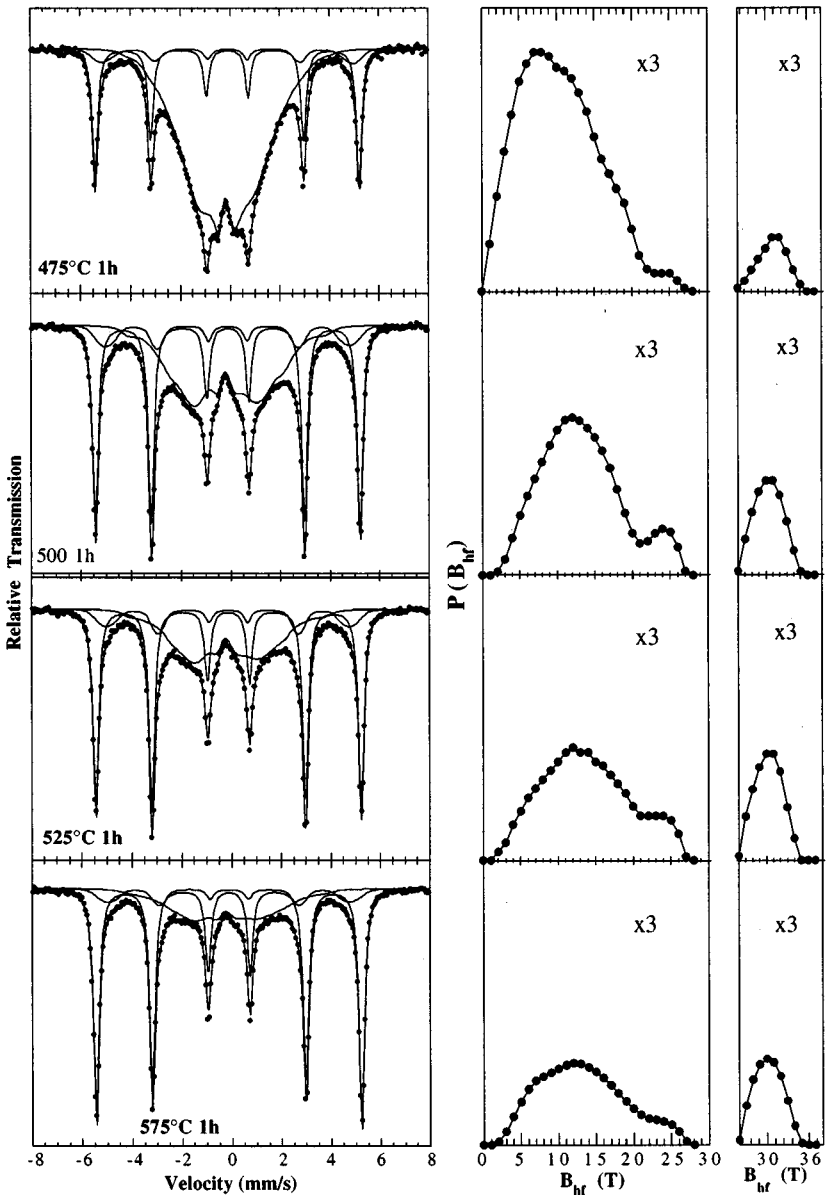

FIG. 5. Mössbauer spectra and fittings for the samples annealed at 475, 500, 525, and 575 °C. The hyperfine-field distributions of the remaining amorphous phase and the 30 T contribution (see text) are given on the right-hand side.

where B_0 is the lowest value for the hyperfine field distribution and j runs over the allowed range of $B_{\rm hf}$.

(b) In the samples with small crystalline fractions (samples annealed at 375, 425, 450 °C 1 h) a crystalline sextet, with a linewidth greater than that of the α-Fe foil, has been used for fitting the bcc-Fe subspectrum and a $P(B_{\rm hf})$ for the remaining amorphous phases, which have Curie temperatures above 290 K.

(c) For samples with larger crystalline fractions a high-field component of the $B_{\rm hf}$ around 30 T is clearly evident in addition to the magnetic sextet attributed to the bcc-Fe crystalline grains. This component increases with the crystallization, suggesting the existence of a relation with the crystalline phase. This contribution evolves in a different way from the amorphous phase. Therefore, two different $P(B_{\rm hf})$, and a crystalline sextet for the bcc-Fe contribution, have been used. This permits the introduction of different relationships between δ and $B_{\rm hf}$ [Eq. (1)] for each distribution and the independent evaluation of the two contributions. The limits of these distributions have been chosen to be equal for all the samples: from 25–37 T for the 30 T contribution and from 0–28 T for the amorphous phase. These are similar to those chosen by other authors[9] for fitting this kind of sample. With these limits we obtained a continuous and smooth evolution of the amount of both contributions as the crystallization proceeds. Moreover hyperfine parameters such as $\langle B_{\rm hf}\rangle$ and $\langle\delta\rangle$ are almost constant for the 30 T contribution (see Table I).

In order to take into account the anisotropies induced by the sample obtainment procedure and by the thermal treatments, the intensity radio of the second to the third line was allowed to vary in the fittings. The obtained value for the as-quenched sample is 2.8, decreasing down to 2.4 as the annealing temperature increases, in agreement with a magnetization which evolves from in plane to a random distribution.

TABLE I. Hyperfine-field parameters and relative Fe percentage (%) in each subspectrum obtained from the Mössbauer spectra for the samples annealed at the indicated temperatures. B_{hf} and $\langle B_{hf}\rangle$ are the hyperfine field and the average of the hyperfine field, respectively: The isomer shift and the average of the isomer shift (δ and $\langle\delta\rangle$) are taken with respect to an α-Fe calibration foil measured at room temperature. The parameter α is that given in Eq. (1). Uncertainties for the last significant figure are given in brackets.

		Amorphous phase			
T_{ann} (°C)	%	$\langle B_{hf}\rangle$ (T)	δ (mm/s)	α	$\langle\delta\rangle$ (mm/s)
as-quenched	100.0	5.5 (2)	−0.11(1)	0.007(1)	−0.07(1)
350	100.0	4.6 (3)	−0.11(1)	0.009(1)	−0.07(1)
375	99.0 (2)	5.1 (1)	−0.11(1)	0.006(1)	−0.07(1)
425	95.5 (2)	5.4 (2)	−0.11(1)	0.007(1)	−0.07(1)
450	94.1 (2)	6.0 (1)	−0.11(2)	0.005(1)	−0.08(2)
475	72.6 (3)	10.5 (1)	−0.13(1)	0.006(1)	−0.07(1)
500	44.4 (7)	13.3 (1)	−0.16(1)	0.005(1)	−0.09(1)
525	35.6 (7)	13.9 (2)	−0.20(2)	0.007(1)	−0.10(2)
575	25.9 (3)	13.2 (3)	−0.21(1)	0.007(2)	−0.14(1)

	α-Fe phase			Interphase			
T_{ann} (°C)	%	$\langle B_{hf}\rangle$ (T)	δ (mm/s)	%	$\langle B_{hf}\rangle$ (T)	$\langle\delta\rangle$ (mm/s)	α
375	1.0 (2)	32.1 (1)	0.04 (2)				
425	4.5 (2)	32.8 (1)	−0.01 (1)				
450	5.9 (2)	32.9 (1)	0.00 (1)				
475	21.3 (3)	32.9 (1)	0.00 (1)	6.1 (3)	31.0 (1)	0.01 (1)	−0.009 (3)
500	44.2 (7)	33.0 (1)	0.00 (1)	11.5 (7)	30.4 (2)	0.00 (1)	−0.009 (3)
525	51.9 (7)	33.1 (1)	0.00 (1)	12.5 (7)	30.2 (2)	−0.01 (1)	−0.007 (3)
575	63.7 (3)	33.1 (1)	0.00 (1)	10.4 (3)	30.2 (2)	0.01 (1)	−0.002 (2)

The amount of Fe in each phase has been obtained from the resonant area of the different contributions, assuming the same recoil-free fraction in all cases. These values and the hyperfine parameters obtained in the fit are shown in Table I. Both the percentage of the bcc crystalline phase and that of the 30 T contribution increase with the annealing temperature, but not in the same proportion. This fact will be discussed in Sec. IV.

The $P(B_{hf})$ corresponding to the sample annealed at 350 °C 1 h is narrower than that corresponding to the as-quenched one, and the average value of B_{hf} ($\langle B_{hf}\rangle$) has decreased. The $P(B_{hf})$ becomes broader when the crystallization has begun and further broadens as it progresses. A small shoulder appears at 10 T and a new contribution at 24 T also appears in the $P(B_{hf})$ corresponding to the sample annealed at 475 °C. These contributions persist in the $P(B_{hf})$ of the samples treated at higher temperatures, together with a continuous increase of $\langle B_{hf}\rangle$.

C. Magnetic measurements

The T_c values of these samples are very sensitive to the external applied field.[18,19] Therefore, in order to avoid field effects, the lowest possible external fields have been used. The T_c value for each sample was obtained from the derivative of the $M(T)$ curves (see Figs. 6 and 7). This gives a sharp minimum in samples annealed at low temperatures where the T_c is well defined.

The T_c of the sample annealed at 350 °C (295 K) shows a decrease with respect to the as-quenched sample (298 K). This fact agrees with the observed decrease of $\langle B_{hf}\rangle$. However, in the sample annealed at 375 °C, where the crystallization process has begun, the T_c of the amorphous phase starts increasing and continues to do so as the crystallization proceeds. The $M(T)$ curves also show that the magnetization drop at the T_c of the amorphous phase becomes smoother as the crystallized fraction increases. This suggests that the Curie temperature of the amorphous matrix is not unique, and there is a distribution of Curie temperatures. In this case, changing the sign of the derivative of $M(T)$ and normalizing, we obtain the distribution of T_c rather accurately. The low field used in the measurements gives very narrow peaks when the T_c is well defined. We have considered the average temperature of the distributions as the representative T_c of these samples.

IV. EVOLUTION OF THE NANOCRYSTALLINE PHASE

In the hyperfine field, there is a 30 T feature associated with the crystalline phase; this is in addition to the well known 33 T sextet of α-Fe. This contribution appears in the Mössbauer spectra of the most of the FeZrB nanocrystalline alloys[20,21] and there are two differing opinions as to the explanation of the origin of this contribution. Some authors, using Mössbauer spectroscopy and analyzing the lattice parameters of highly crystallized FeZr samples,[22,23] conclude that the crystalline phase is a bcc-FeZr solid solution containing 3–4 at. % of Zr. The 30 T contribution is then interpreted as arising from the Fe atoms with at least one nearest-neighbor Zr atom. Other authors compare the Mössbauer spectra of the FeZr crystallized alloys with those of FeTiCuB and FeNbCrCuB crystallized alloys.[24] The spectra of all of them present a 30 T contribution, these they attribute to the contribution of a crystal-amorphous interphase region.

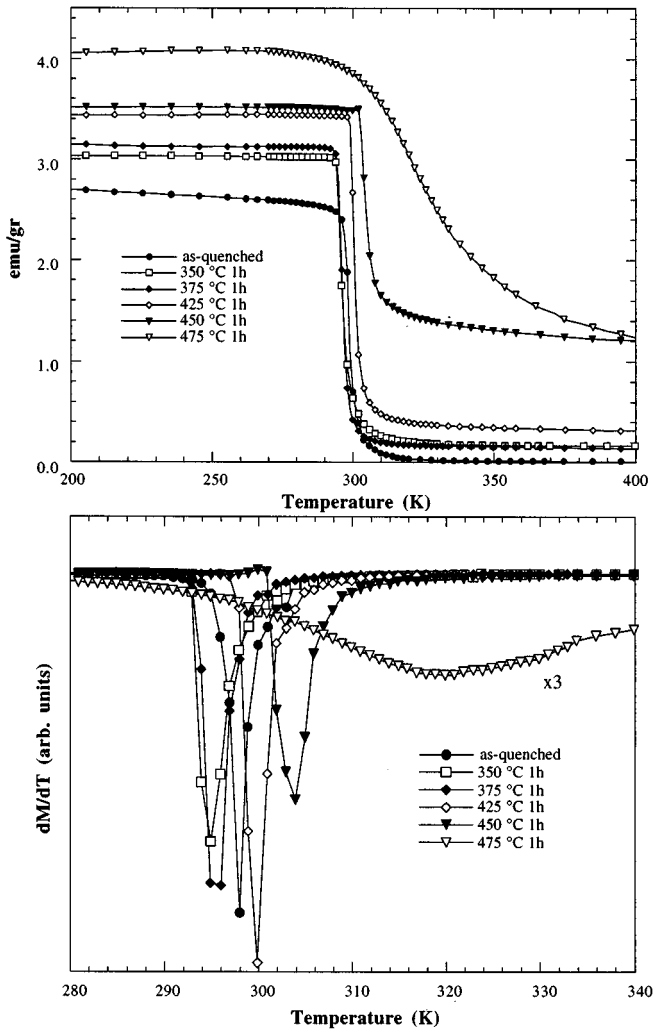

FIG. 6. (a) Thermomagnetic $M(T)$ curves with an external applied field of 5 G for the samples annealed at temperatures indicated in the figure. (b) Derivatives (dM/dT) of the $M(T)$ curves.

From Fig. 3(a), we can observe the evolution of the lattice parameter for the crystalline phase as a function of the annealing temperature. The calculated values are slightly higher than that of the Fe foil which could suggest the presence of a small amount of Zr atoms in the Fe lattice (Zr atoms have a larger radius than the Fe atoms). Nevertheless, taking into account the experimental errors, we cannot state this for certain, since the Fe-foil lattice parameter is within the experimental error of the lattice parameter for the crystalline phase. In Fig. 3(b), we show the evolution of the Fe percentages for both the crystalline phase and the 30 T contribution (which we denote as the interphase in the figure and hereafter). These increase with the annealing temperature but not in same proportion. The crystalline phase displays a continuous increase while the 30 T contribution region stops growing, and further on the annealing sequence, shows a decrease in the latter stages of the crystallization process. If the 30 T contribution of the spectra is due to the presence of Zr in the bcc crystalline phase, both percentages would have to exhibit the same evolution with the annealing temperature. Therefore, we must conclude that the presence of Zr is not,

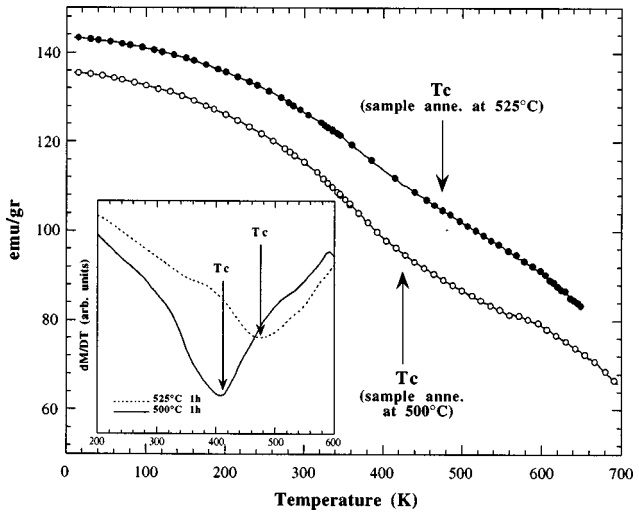

FIG. 7. $M(T)$ curves at external field applied of 800 G of the amples annealed at 500 and 525 °C. The inset shows the derivaves of the $M(T)$ curves.

pparently, the origin of the 30 T contribution in the Mössauer spectra.

Recently Del Bianco *et al.*[25] have reported a Mössbauer tudy of nanocrystalline ball-milled pure iron. They associate crystalline interfacial region at the grain boundaries with a 6 T contribution in the spectra. In FeZr nanocrystalline alys the values of $\langle B_{nf} \rangle$ and δ (30 T and -0.1 mm/s, respecvely) suggest that the Fe atoms which produce this contriution should belong to the amorphous-crystal interphase egion. Assuming the crystals form spherical grains[26] and sing the grain sizes obtained from x-ray diffraction data Fig. 3(a)], we can compare the crystallized fraction with the increase in grain size. Following these arguments, we see that from the sample annealed at 500 °C and above, the increase of the crystallized fraction is due only to the crystalline growth and not to new nucleation sites. So, if we assume that the 30 T contribution is due to the interphase region, this could explain the saturation and eventual decrease of this region in the sample annealed at 575 °C as the grains begin to come into contact one another. In terms of the number of atomic layers corresponding to the interphase, Table II shows that the interphase region would be formed by about 2

TABLE II. Comparison of the relative Fe percentages for the α-Fe and the interphase regions as taken from the x-ray and Mössbauer results for various annealing temperatures, as indicated. For the Mössbauer results these have been taken from the fitting parameters, while the x-ray values are calculated from the gain size. A 3% uncertainty applies to all figures.

	Measured (Mössbauer)		Calculated (from grain size)			
T_{ann} (°C)	α-Fe	interphase	α-Fe	surface+ one layer	α-Fe	surface+ two layers
475	77	23	79	21	72	28
500	79	21	86	14	80	20
525	81	19	87	13	82	18
575	86	14	88	12		

atomic layers for the samples annealed at 475, 500, and 525 °C and 1 to 2 layers for the sample annealed at 575 °C. This strongly supports the conclusion that the 30 T contribution to $P(B_{hf})$ is produced by a disordered interphase region around α-Fe crystallites.

In Table I, we display the fitting parameters used in the Mössbauer spectra for the various phases with the corresponding annealing temperature. From this we see that the B_{hf} value of the bcc-Fe phase increases with the annealing temperature and is below the expected value of 33 T for the samples with small crystalline fractions. Recently, Greneche *et al.* have observed a similar effect in nanocrystallized FeCrCuNbSiB alloys.[8] In these samples, the B_{hf} of the crystalline phase displays a decrease above the T_c of the amorphous phase. We can compare this effect with that observed in our partially crystallized $Fe_{87}Zr_6CuB_6$ samples. In our case, the Mössbauer spectra have been obtained at 290 K, only 5 K below the T_c of the sample treated at 375 °C. This causes a decrease of the hyperfine field of the nanocrystals, since the T_c of the amorphous phase increases with the annealing temperature and then the B_{hf} of the crystalline phase should return back to the normal value of 33 T, as is observed for the sample annealed at 525 °C.

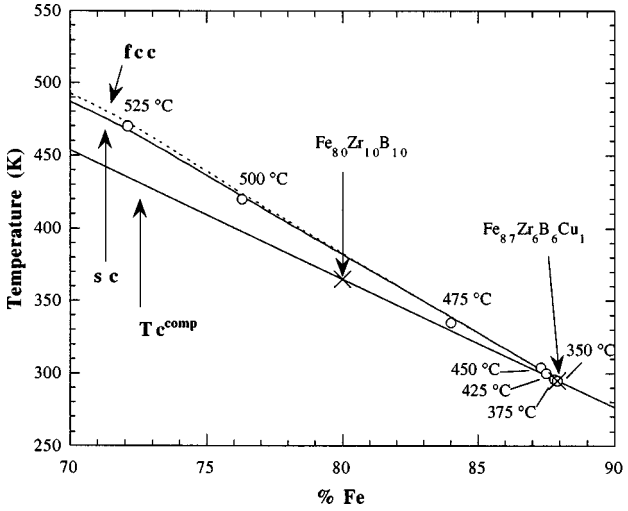

FIG. 8. Evolution of the remaining amorphous phase T_c for the annealed samples with respect to the Fe content (open circles). The T_c values have been obtained from the derivative of the $M(T)$ curves. The continuous line indicates the T_c evolution of the $Fe_{100-2x}Zr_xB_x$ amorphous alloys. The solid and dashed lines indicate the variations expected from the models of crystallite ordering for the sc and fcc arrangements, respectively. See text.

V. EVOLUTION OF THE AMORPHOUS PHASE AND EXCHANGE-FIELD PENETRATION

A. Curie temperature

A small decrease in Curie temperature and $\langle B_{hf} \rangle$ values of the samples annealed at 350 and 375 °C with respect to the as-quenched sample (Table I) is observed. This fact can be associated with the relaxation of the amorphous alloys and related with the decrease of the average interatomic distances. This behavior is in sharp contrast with the increase of T_c upon annealing observed in other Fe-rich amorphous alloys.[27] However, FeZr and FeZrB alloys show INVAR behavior (see Ref. 27, p. 292) and thus a decrease of T_c under pressure (or an increase of T_c upon expansion) as has been reported in Refs. 28 and 29. This has been explained as a consequence of the increase of the density of states with increasing volume which overcomes the small decrease in exchange interaction as the Fe-Fe distance increases.[30] The observed behavior of T_c upon annealing is then in agreement with the pressure effects previously reported.[28]

In Fig. 6 we show the thermomagnetic measurements as a function of the sample annealing temperature. A progressive increase of T_c for the amorphous phase is observed upon crystallization. Samples with less than 10% crystallized fraction show a sharp transition at T_c. At the early stages of the crystallization process (α-Fe$<$10%) there is a very small quantity of amorphous phase around the nanocrystallites and the influence of these on the amorphous phase is, on average, very low, so that the magnetic changes of the amorphous phase will be mainly due to composition changes. If copper and iron are segregated from the amorphous matrix, the latter retains the composition $Fe_{100-2x}Zr_xB_x$. Recently, Barandiaran *et al.*[30] have reported T_c values of some Fe-rich FeZrB alloys. A linear increase of the T_c values with the relative decrease of the Fe concentration in the remaining amorphous phase is observed. Figure 8 shows the T_c for the amorphous phases in the annealed samples as a function of the composition, which has been deduced by assuming that the nanocrystals and the interphase region are composed solely of iron. The straight line is an extrapolation from T_c data of the $Fe_{87}Zr_6CuB_6$ (from the present study) and $Fe_{80}Zr_{10}B_{10}$ amorphous alloys taken from Ref. 30. We can observe that in the very early stages of the crystallization, the T_c of the remaining amorphous phases are very close to the expected values, and therefore, they can be determined simply from compositional considerations.

In the $M(T)$ curves for the samples annealed at 475, 500, and 525 °C, shown in Figs. 6 and 7, a smooth transition appears at the T_c with the increase of the crystallized fraction. At these stages of the crystallization process, the remaining amorphous phase is no longer magnetically homogeneous, but presents a distribution of Curie temperatures,[7] and the T_c values in these samples progressively depart from the expected values (Fig. 8). This fact is frequently observed in these kinds of samples. Some authors account for such a behavior by assuming an exchange-field penetration of the α-Fe nanocrystals into the amorphous matrix.[6,14] This field decays exponentially with the distance from the crystal surface l as

$$H = H_0 \exp(-l/\lambda), \tag{2}$$

where λ is a penetration depth characteristic of the material. As a consequence, the Curie temperature of these amorphous layers will increase in proportion to the local molecular field and, on average, the T_c of the amorphous phase increases above the expected value. Furthermore, as a consequence of the spatial variation of the exchange field, a distribution of T_c appears in the amorphous matrix. The volume of the nearest layers adjacent to the α-Fe crystals increases with the crystal grain size and, therefore, the effect of the exchange-field penetration of the α-Fe crystals extends over a larger

amorphous volume. Consequently, the average T_c of the amorphous phase continues to increase and the T_c distribution grows broader.

In some papers, the exchange-field penetration effect on the amorphous matrix is discussed based on the average intercrystalline distance.[6,26] The distribution of the crystals inside the amorphous matrix is normally assumed to form a regular array of cubic crystals. In this case the crystallites will only come into contact with each other when the sample is fully crystallized. Therefore, the calculated intercrystalline distances using this assumption are not the most suitable for the discussion of this effect. Assuming an ordered distribution and uniform growth of spherical nanocrystals (as is observed by electron microscopy[26]), all having roughly the same radius, inside the amorphous matrix, we can evaluate the effect of field penetration quantitatively. We shall assume that the nanocrystallines form a cubic ''mesh'' somewhere between two different arrangements: the least dense simple cubic order (sc), and the most dense face centered cubic one (fcc) [see Fig. 9(a)]. The minimum distance between crystals d for each arrangement can be calculated by means of the following relationships:

$$d=\begin{cases} D[(\pi/6x)^{1/3}-1] & \text{for sc order,} \\ D[(\sqrt{2}\pi/6x)^{1/3}-1] & \text{for fcc order,} \end{cases} \tag{3}$$

where D represents the grain size of the crystals and x the crystalline volume fraction. Therefore, the ''mesh'' parameters will be $d+D$ and $\sqrt{2}(d+D)$ for the sc and fcc orders, respectively. Now we can calculate the distribution of the remaining amorphous phase as a function of the distance from the surface of the crystals (see the Appendix for details). The results of these calculations are shown in Fig. 9(b).

In the sc order, there would be less than 4% of the amorphous phase at a distance of 2 nm from the crystalline surfaces for the sample annealed at 450 °C but more than 40% for the sample annealed at 525 °C. In the fcc order, at the same distance and for the sample annealed at 450 °C, there would be the same percentage of the amorphous phase as in the sc case, but for the sample annealed at 525 °C the percentage would go up to 55%. This increases up to 80% of the amorphous phase if we make the evaluation at a distance of 3 nm. Therefore, in the samples with small crystalline volume fractions, only a small quantity of the amorphous phase would be affected by the nanocrystals, but when the crystalline volume fractions are higher, most of the remaining amorphous phase would be under the influence of the crystallites. At that point, the magnetic properties of the amorphous phase are strongly governed by the crystalline exchange field and the difference of T_c for this phase with respect to the expected one, based on compositional considerations only, is significant.

The amorphous region at a ''large'' distance from the crystals would not feel the exchange field, and the T_c would be simply that corresponding to the mean composition (T_c^{comp}). Considering, then, a direct relation between the exchange field at a given point and the T_c in the amorphous matrix, we find an exponential decrease of the T_c of the amorphous phase with the distance from the crystalline surface, which falls as

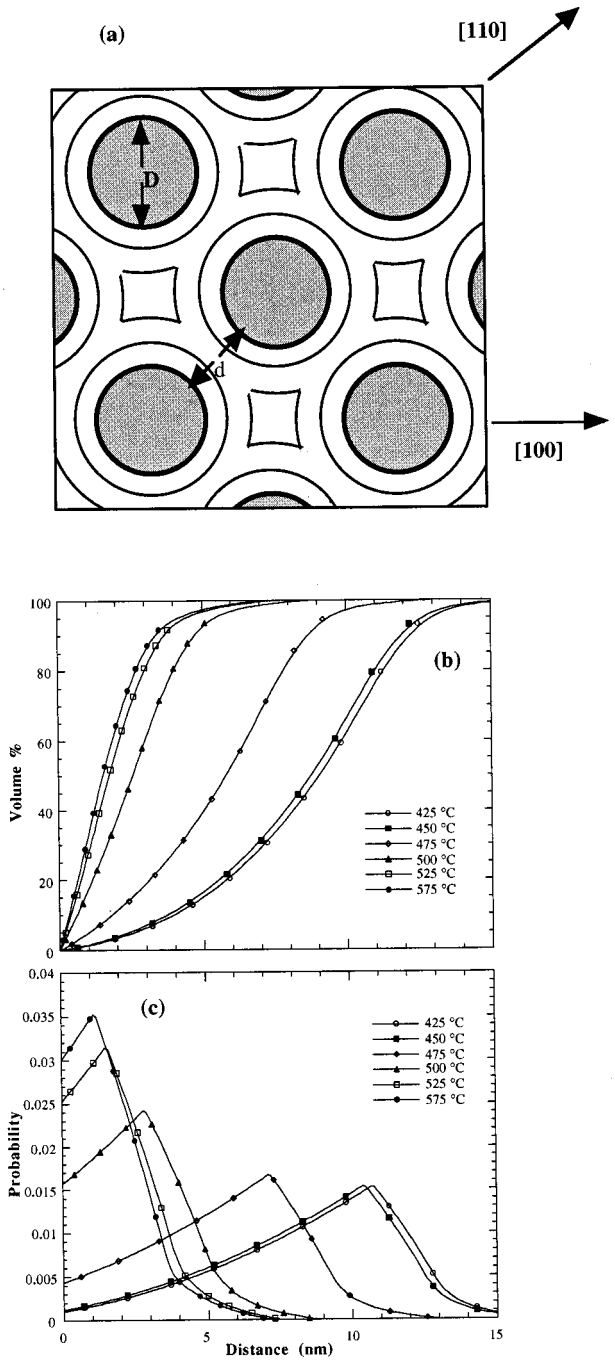

FIG. 9. (a) Schematic representation of the face centered cubic crystallite arrangement in the amorphous matrix. D represents the grain size of the crystalline phase and d the minimum distance between crystals. (b) Volume distribution of the remaining amorphous phase with respect of the distance from the surface of the crystals for the fcc arrangement of the crystals, the annealing temperatures are indicated. (c) Volume distribution probability dV/dl for the remaining amorphous phase as a function of the distance from the surface of the crystals.

$$T_c(l)=\begin{cases} T_c^{\text{Fe}}e^{-l/\lambda} & \text{when } T_c^{\text{Fe}}e^{-l/\lambda}>T_c^{\text{comp}}, \\ T_c^{\text{comp}} & \text{when } T_c^{\text{Fe}}e^{-l/\lambda}<T_c^{\text{comp}}, \end{cases} \tag{4}$$

where T_c^{Fe} is the Curie temperature of the α-Fe phase, and l is the distance from the crystalline surface into the amorphous phase.

TABLE III. Atomic percentage of the interphase region obtained from the fittings results of the Mössbauer spectra and from the model developed in this paper (sc indicates simple cubic arrangement of the crystals and fcc face centered cubic). The interphase region is assumed to be 6 Å thick. A 1% uncertainty applies to all figures.

T_{ann} (°C)	Mossbauer	sc model	fcc model
475	5	5	5
500	10	8	9
525	11	11	12
575	9	10	11

Not all the T_c values obtained from Eq. (4) have the same probability or weight in the distribution. Their probabilities will be related to the quantity of the amorphous phase at the distance l. From the distribution of the amorphous phase given in Fig. 9(b), we can calculate the distribution of T_c as

$$D(T_c)=T_c(l)\,\frac{dV}{dl}, \tag{5}$$

where dV/dl represents the volume distribution of the remaining amorphous phase, that is, the volume probability of amorphous phase with regard to the distance from the crystalline surfaces [Fig. 9(c)]. Averaging expression (5) we obtain the average T_c $\langle T_c\rangle$ for the remaining amorphous phase as

$$\langle T_c\rangle=\frac{\int T_c(l)\,\frac{dV}{dl}\,dl}{\int \frac{dV}{dl}\,dl}. \tag{6}$$

All the parameters related with Eq. (5) have been obtained experimentally with the exception of the penetration length λ. Several authors[31,32] estimate that the value of λ should be between 1 and 2 atomic distances, i.e., between 3 and 6 Å. The values of $\langle T_c\rangle$ corresponding to $\lambda=5$ Å are shown in Fig. 8 for both the sc and fcc ordering regimes. These are compared with the T_c^{comp} values. With a λ value of 5 Å, the exchange-field penetration is effective only in the first four to five atomic layers, so the grain size plays a very important role. A simple calculation shows that for the same crystalline volume fraction, the volume of the amorphous phase at a distance of 1 nm from nanocrystals with $D=10$ nm is more than twice the quantity surrounding nanocrystals with $D=20$ nm. In Ref. 6, Hernando *et al.* show that for the partially crystallized $Fe_{77}B_{18}Nb_4Cu$ samples, with a grain size of 10 nm, the Curie temperatures are 100 K higher than those corresponding to the T_c^{comp}. Our samples present grain sizes of 20 nm and the observed differences are only about 40 K.

With respect to the interphase, if we assume that this region is a 6 Å (two atomic distances) thick, we can calculate, from the model, the atomic percentage that this region represents for the different samples. Table III shows these percentages and compares them with those obtained from the fitting results of the Mössbauer spectra. Both percentages are quite close and show the same trend, that is, an increase with the annealing temperature up to 525 °C, and then a decrease. This last decrease is due to the overlapping of the interphase regions when the crystallites approach each other, as it has been commented on above.

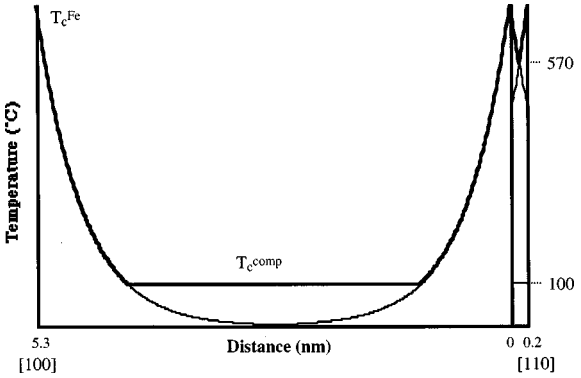

FIG. 10. Schematic representation of the calculated T_c distribution from the exchange-field penetration in the remaining amorphous phase of the $Fe_{85}Zr_7B_6Cu_2$ sample with a crystallized fraction of 70%. An fcc arrangement of the crystallites has been assumed. Taking 0 as the position at the crystallites surface, and crossing the crystallite mesh in the [110] direction, we meet the nearest-neighbor crystallite a distance 0.2 nm away, while in the [100] direction, we encounter the nearest crystallite a distance 5.3 nm away. The lines then indicate the variation of the amorphous phase T_c between these points. See text.

B. Temperature dependence of the coercive field

Changes of the coercive field with temperature in the nanocrystalline samples are related to the T_c of the amorphous phase. The extremely small coercive field of these samples is due to the exchange coupling among the crystals, which is effective, provided that the amorphous matrix is ferromagnetic. When the temperature reaches the T_c of the amorphous matrix, the coercive field sharply increases with the temperature. However, this increase becomes smoother and smoother as the crystalline volume fraction of the sample grows. For instance, in the $Fe_{85}Zr_7B_6Cu_2$ sample with a volume crystalline fraction of about 70%, Slawska-Waniewska *et al.*[26] observe a difference of about 400 °C between the Curie temperature of the amorphous phase, as estimated from the composition, and the temperature at which the coercive field exhibits a maximum value. This occurs at about 500 °C.[26] We can calculate the T_c distribution between the nearest crystalline neighbors by means of the model discussed in the previous section using Eqs. (2) and (3). With the reported grain size of 12 nm, and using a fcc arrangement of crystalline spheres, the T_c distribution for $\lambda=5$ Å is as shown in Fig. 10. As can be seen, there are different distances between the nearest crystalline neighbors depending on the direction considered in the crystallite mesh. Therefore, we can expect different T_c distributions for the various directions. The largest distance between the crystals is presented in the [100] direction, that is, 5.3 nm. In this direction, the T_c of the central amorphous zone would be the compositional one. In contrast, in the [110] direction, with an intercrystalline distance of only 0.2 nm, all of the amorphous phase between the nearest neighbor crystallites is under the exchange field influence, see Fig. 10. From this figure, when the temperature reaches 100 °C, i.e., the T_c^{comp} of the amorphous matrix, the amorphous phase of central zone located between the crystallites at the corners becomes paramagnetic. So, in the [100] direction of the crystalline mesh, the crystals begin to decouple and, consequently, the coercive

field begins to increase. As the temperature continues to increase, more of the amorphous phase becomes paramagnetic, thus the crystals become magnetically more isolated and the coercive field would further continue to increase. When the temperature reaches the T_c of the amorphous phase situated under the exchange field influence in the [110] direction, the crystals become completely isolated and the coercive field is expected to reach its maximum value, this occurs at about 570 °C.

According to the model, the coercive field for samples with small crystalline fractions should exhibit a sharp increase when the temperature reaches the T_c^{comp} of the remaining amorphous phase; the maximum would be at few degrees above T_c^{comp}. However, in samples with larger crystalline fractions, this maximum would be at the Curie temperature of the amorphous phase located between the nearest crystals, which is much larger than the compositional one.

C. Hyperfine field distribution

Figures 4 and 5 show the hyperfine field distributions $P(B_{\text{hf}})$ of the amorphous phase for the samples studied. A narrowing of the $P(B_{\text{hf}})$ is observed in the sample annealed at 350 °C, with respect to the as-quenched sample. As we have already commented, this fact is due to a structural relaxation process that induces a decrease in the T_c of the as-quenched sample. In the partially crystallized samples (where $T_{\text{ann}} \leqslant 475$ °C), the $P(B_{\text{hf}})$ of the amorphous phase is narrow, but shows a small tail towards higher hyperfine fields.

Taking into account the sensitivity of the B_{hf} to local magnetic environments, the influence of the crystalline exchange field penetration may also be reflected in the $P(B_{\text{hf}})$. The appearance of the tail in the $P(B_{\text{hf}})$ with the crystallization process could be a consequence of this influence. The tail corresponds to the part of the amorphous phase under influence of the nanocrystals. These would produce an increase in the B_{hf} of the amorphous phase nearest to the crystallites due to the presence of the higher crystalline exchange field. As there is more amorphous phase influenced by the crystals with further annealing, the high field tail grows in importance with respect to the total distribution.

The maximum of the $P(B_{\text{hf}})$ is at 3–4 T for the partially crystallized samples with $T_{\text{ann}} \leqslant 450$ °C, however, this shifts to 7 T for the sample annealed at 475 °C. This increase is a consequence of the compositional changes in the amorphous phase which also increases the T_c^{comp} for this phase.

The $P(B_{\text{hf}})$ of the sample annealed at 475 °C shows a small shoulder at 10–11 T. This shoulder becomes the main contribution in the $P(B_{\text{hf}})$ for the amorphous phase of the samples annealed at higher temperatures. At the same time, a new contribution located at about 23–24 T appears in the $P(B_{\text{hf}})$ of the amorphous phase. This contribution remains in the $P(B_{\text{hf}})$ of samples with larger crystalline volume fractions. These facts indicate that at these stages of the crystallization process, the remaining amorphous phase presents compositional inhomogeneities which accentuate as the crystallization process advances. This inhomogeneity is related to the fact that the different components of the amorphous phase have different diffusion coefficients. For the sample annealed at 475 °C, there is a crystallized fraction of about 19%. Even at this early stage in the crystallization process, there has been sufficient diffusion such as to leave the amorphous phase inhomogeneous.

Miglierini *et al.*[33] associate the 23–24 T contribution with an extension of the interphase region to lower hyperfine fields. However, this contribution does not evolve upon annealing in the same way as the contribution of the interphase, but presents different relative increases of probability in the $P(B_{\text{hf}})$ of the samples containing higher crystallized fractions. Nevertheless, from the values in Table I, we can see that the isomer shift (δ) associated with the hyperfine fields of the 23–24 T (−0, 16 mm/s) contribution has no continuity with those associated to the hyperfine fields of the interphase. Both the main contribution (10–11 T) and that at 23–24 T could be due to zones with definite but different short range order in the amorphous matrix which correspond to regions with a composition similar to the phases appearing in the second stage of crystallization (Fe_3Zr, Fe_2B, Fe_2Zr). This is supported by recent studies of the temperature evolution of partially crystallized FeZrB, as evidenced by Mössbauer spectroscopy.[33,34] In Ref. 34, the authors observe a contribution to low hyperfine fields (8–10 T) in the spectra which are associated with an Fe_3Zr-like phase with a $T_c = 550$ K. Furthermore, the hyperfine fields of crystalline Fe_2B and Fe_3Zr are known to be about 27 and 14 T, respectively.[14] Therefore, we can associate the 10–11 T contribution to an amorphous region with Fe_3Zr-like short range order (SRO) and the 23–24 T contribution to the region with Fe_2B-like SRO.

The broadening of the $M(T)$ curves in the region of the Curie temperature of the amorphous phase would also be favored by such inhomogeneities. This broadening appears at the same annealing temperature (475 °C) in both the $M(T)$ curves and $P(B_{\text{hf}})$. The drop in the magnetization [in the $M(T)$ curve], of the 475 °C annealed sample begins before the T_c of the sample annealed to 450 °C. This indicates a high degree of inhomogeneity at this stage, see Fig. 6. Therefore, the amorphous phase can no longer be defined as a single magnetic phase, but is quite inhomogeneous, as evident in the hyperfine-field distribution from the Mössbauer measurements and $M(T)$ curves. Nevertheless, at this stage of the crystallization process, most of the amorphous phase is strongly influenced by the Fe crystalline phase and, therefore, the amorphous phase T_c is governed by the crystalline exchange-field penetration. In this sense the inhomogeneities would have little influence on the average T_c of the amorphous remaining matrix, which explains the agreement between the model and the experimental $\langle T_c \rangle$.

VI. CONCLUSIONS

The crystallization process of the $Fe_{87}Zr_6B_6Cu$ sample has been studied by means of x-ray diffraction, Mössbauer spectroscopy, and magnetic measurements. The experimental results shows an Fe-rich region is formed as an interphase around the α-Fe nanocrystals. This interphase is highly disordered and extends to one to two atomic layers from the crystallites into the amorphous phase.

The T_c of the amorphous phase increases during the crystallization. This increase is due to two factors: (i) the compositional changes in the amorphous phase and (ii) the crys-

talline exchange-field penetration. For the samples with less than 10% crystalline fraction, the dominating factor determining the T_c increase is due to compositional changes in the amorphous matrix. For samples with larger crystalline fractions, the T_c of the remaining amorphous phase departs progressively from the compositional values to those predicted by the model presented, indicating the increasing influence of the exchange-field penetration.

The effects of the exchange-field penetration on the remaining amorphous phase have been evaluated by means of a simple model. This model proposes a direct relationship between exchange field penetration and the T_c of the amorphous atomic layers. The model assumes that the T_c falls exponentially from the crystalline value at the crystal boundary, to that corresponding to the composition of the amorphous phase at a distance determined by the penetration length λ of the amorphous phase. This model has been applied to two systems (partially crystallized $Fe_{87}Zr_6B_6Cu$ and $Fe_{77}B_{18}Nb_4Cu$ alloys) with different grain sizes and compositions. The calculated average T_c values are in very good agreement with the measured ones. The value of the field penetration length is about 5 Å, in agreement with the expected value.

The changes of the coercive field with the temperature in the nanocrystalline samples have also been evaluated by the model. The model predicts that the coercive field begins to increase when the temperature reaches the T_c corresponding to the composition of the amorphous phase, and shows a maximum of H_c at the temperature where the grains become exchange isolated, since the intervening amorphous phase between the nearest-neighbor crystallites becomes paramagnetic.

The changes in the hyperfine-field distributions of the amorphous phase are due to the appearance of magnetic and composition inhomogeneities. The magnetic inhomogeneities are induced by the crystalline exchange-field penetration and are reflected in the $P(B_{\mathrm{hf}})$ by tails extending towards high fields. When the crystallization process is advanced, new contributions at 11 and 23 T appear in the $P(B_{\mathrm{hf}})$ of the amorphous matrix. These contributions are related to zones in the remaining amorphous matrix with short range order similar to the crystalline phases which will appear at the secondary crystallization. The inhomogeneity is also reflected in the $M(T)$ curves, which give T_c distributions which, for the samples annealed at 475 °C and above, show a broadening with respect to the samples annealed at lower temperatures.

ACKNOWLEDGMENTS

This work was supported by the Spanish CICYT under Grant No. MAT 96/1023. J.S.G. and D.S.S. would like to thank the Basque Government for financial support. The authors also acknowledge Professor A. Hernando for useful discussions and Dr. P. Gorria (University of Oviedo) and Dr. L. Fernández Barquín (University of Cantabria) for preparation of the amorphous ribbons.

APPENDIX

If we assume simple cubic and face centered cubic arrangements of spheres with an interspherical distance d, see Fig. 9(a), the volume occupied in a cube by the spheres with respect to the radius r of the spheres can be calculated using the following relations.

(1) For a simple cubic arrangement

$$V=\begin{cases} \dfrac{4}{3}\,\pi r^3 & \text{when } r\leqslant d, \\ 6\pi d\left(r^2-\dfrac{d^2}{3}\right)-\dfrac{8}{3}\,\pi r^3 & \text{when } d\sqrt{2}>r>d. \end{cases}$$

(2) For a face centered cubic arrangement.

$$V=\begin{cases} 4\left(\dfrac{4}{3}\,\pi r^3\right) & \text{when } r\leqslant d, \\ 48\pi d\left(r^2-\dfrac{d^2}{3}\right)-\dfrac{80}{3}\,\pi r^3 & \text{when } \dfrac{d\sqrt{3}}{3}>r>d. \end{cases}$$

Using the above equations, 96.51 and 96.41 % of the volume of the cube can be evaluated for sc and fcc, respectively. Therefore we find that the distribution of the volume in the cube, with respect to the distance from the surface of the spheres (*1*), can be calculated as follows:

$$V(l)=V(r)-V\left(\frac{D}{2}\right).$$

[1] Y. Yoshizawa, S. Oguma, and K. Yamauchi, J. Appl. Phys. **64**, 6044 (1988).

[2] G. Herzer and H. Warlimont, Nanostruct. Mater. **1**, 263 (1992).

[3] J. M. Barandiaran, L. Fernández Barquín, J. C. Gómez Sal, P. Gorria, and A. Hernando, Solid State Commun. **88**, 75 (1993).

[4] P. Gorria, J. S. Garitaonandia, and J. M. Barandiarán, J. Phys.: Condens. Matter **8**, 5925 (1996).

[5] G. Herzer, IEEE Trans. Magn. **25-5**, 3327 (1989).

[6] A. Hernando, I. Navarro, and P. Gorria, Phys. Rev. B **51**, 3281 (1995).

[7] P. Gorria, J. S. Garitaonandia, and J. M. Barandiarán, Mater. Sci. Eng. A **226-228**, 175 (1997).

[8] J. M. Greneche and A. Slawska-Waniewska, in *Non-crystalline and Nanoscale Materials*, Proceedings of the Fifth International Workshop on Non-crystalline solids, edited by R. Rivas and M. A. Lopez-Quintela (World Scientific, Singapore, 1998), p. 233.

[9] M. Miglierini, J. Phys.: Condens. Matter **6**, 1431 (1994).

[10] T. Pradell, N. Clavaguera, J. Zhu, and M. T. Clavaguera-Mora, J. Phys.: Condens. Matter **7**, 4129 (1995).

[11] G. Rixecker, P. Schaaf, and U. Gonser, J. Phys.: Condens. Matter **4**, 10 295 (1992).

[12] D. S. Schmool, J. S. Garitaonandia, and J. M. Barandiarán, following paper, Phys. Rev. B **58**, 12159 (1998).

[13] P. Duhaj, I. Mat'ko, P. Svec, J. Sitec, and D. Janickovic, Mater. Sci. Eng. B **39**, 208 (1996).

[14] I. Navarro Palma, Ph.D. thesis, Universidad Complutense de Madrid, 1994.

[15] B. D. Cullity, *Elements of X-Ray Diffraction* (Addison-Wesley,

New York, 1960), p. 330.
[16] R. A. Brand, J. Lauer, and D. M. Herlach, J. Phys. F **14**, 555 (1984).
[17] G. Le Caër and J. M. Dubois, Phys. Status Solidi A **64**, 275 (1981).
[18] C. Michaelsen and L. Schultz, Acta Metall. Mater. **39**, 987 (1991).
[19] K. M. Unruh and C. L. Chien, Phys. Rev. B **30**, 4968 (1984).
[20] A. Grabias and M. Kopcewicz, Mater. Sci. Forum **269-272**, 725 (1998).
[21] I. Orue, P. Gorria, F. Plazaola, M. L. Fernández-Gubieda, and J. M. Barandiaran, Hyperfine Interact. **94**, 2199 (1994).
[22] T. Kemény, L. K. Varga, L. F. Kiss, J. Balogh, A. Lovas, and I. Vincze, Mater. Sci. Eng., A **226-228**, 201 (1997).
[23] T. Kemény, L. K. Varga, L. F. Kiss, J. Balogh, T. Pusztai, L. Tóth, and I. Vincze, Mater. Sci. Forum **269-272**, 419 (1998).
[24] M. Miglierini and J. M. Greneche, J. Phys.: Condens. Matter **9**, 2302 (1997).
[25] L. Del Bianco, A. Hernando, E. Bonetti, and E. Navarro, Phys. Rev. B **56**, 8894 (1997).
[26] A. Slawska-Waniewska, P. Nowicki, H. K. Lachowicz, P. Gorria, J. M. Barandiaran, and A. Hernando, Phys. Rev. B **50**, 6465 (1994).
[27] F. E. Luborsky, *Amorphous Metallic Alloys* (Butterworths Monographs in Materials, Butterworths, 1983), p. 174.
[28] J. M. Barandiaran, P. Gorria, I. Orue, M. L. Fernández-Gubieda, F. Plazaola, and A. Hernando, Phys. Rev. B **54**, 3026 (1996).
[29] K. Fukamichi, T. Goto, H. Komatsu, and H. Wakabayashi, in *Physics of Magnetic Materials*, edited by W. Gorzkowsky, H. K. Lachowicz, and H. Szymczak (World Scientific, Singapore, 1989), p. 354.
[30] J. M. Barandiaran, P. Gorria, I. Orue, M. L. Fernández-Gubieda, F. Plazaola, J. C. Gómez Sal, L. Fernández Barquín, and L. Fournes, J. Phys.: Condens. Matter **9**, 5671 (1997).
[31] N. García and A. Hernando, Phys. Rev. B **45**, 3117 (1992).
[32] I. Navarro, M. Ortuño, and A. Hernando, Phys. Rev. B **53**, 11 656 (1996).
[33] M. Miglierini and J. M. Greneche, J. Phys.: Condens. Matter **9**, 2321 (1997).
[34] A. Slawska-Waniewska and J. M. Grenèche, Phys. Rev. B **56**, R8491 (1997).